Eur. Phys. J. B **23**, 79–86 (2001)

THE EUROPEAN PHYSICAL JOURNAL B

EDP Sciences

Rupture energy of a pendular liquid bridge

O. Pitois[1,a], P. Moucheront[2], and X. Chateau[2]

[1] LPMDI, Université de Marne-la-Vallée, bâtiment Lavoisier, 5 boulevard Descartes, Champs-sur-Marne, 77454 Marne-la-Vallée Cedex 2, France
[2] LMSGC, 2 allée Kepler, Cité Descartes, 77420 Champs-sur-Marne, France

Received 18 September 2000 and Received in final form 10 June 2001

Abstract. We propose a simple expression for the rupture energy of a pendular liquid bridge between two spheres, taking into account capillary and viscous (lubrication) forces. In the case of capillary forces only, the results are in accordance with curve fitting expressions proposed by Simons *et al.* [2] and Willett *et al.* [5]. We performed accurate measurements of the force exerted by liquid bridges between two spheres. Experimental results are found to be close to theoretical values. A reasonable agreement is also found in the presence of viscous forces. Finally, for small bridge volumes, the rupture criterion given by Lian *et al.* [10] is modified, taking into account additional viscous effects.

PACS. 68.10.-m Fluid surfaces and fluid-fluid interfaces – 62.10 Mechanical properties of liquids.

1 Introduction

The presence of an interstitial liquid within a granular assembly can have a significant effect on the mechanical behaviour of the medium, with respect to its dry counterpart. The formation of liquid menisci at contacts between grains generally induce capillary forces increasing the strength of the system. For example, the enhancement of the cohesion can have harmful effects on granular flows by jamming the discharge of silos [1]. On the other hand, this binding effect can be beneficial and is used in a wide range of manufacturing processes involving powder granulation. In such dynamic systems, the formation of agglomerates appears to be related to the balance between the rupture energy of liquid bridges and the particles kinetic energy. In addition, the fracturation of the resulting agglomerates involves liquid bridges rupture and its associated rupture energy. Although the behaviour of such particles assemblies is still hardly predictable by means of micro-mechanical models, the knowledge of simple expressions to describe interactions at the microscopic scale is nevertheless of practical interest.

The rupture energy $W_{\rm cap}$ of pendular liquid bridges between spherical particles has been investigated by Simons *et al.* [2–4] in the case of perfect wetting conditions. The authors considered a toroidal bridge geometry and calculated the integral of the quasi-static capillary forces with respect to the separation distance. They obtained a non-trivial integral expression, which was solved in an approximate manner. A simple expression was then derived by curve fitting:

$$\tilde{W}_{\rm cap} = \frac{W_{\rm cap}}{\sigma R^2} \approx c\,\tilde{V}^{0.5} \tag{1}$$

where σ is the surface tension of the liquid / air interface, R is the radius of the spheres, $\tilde{V} = V/R^3$ is the dimensionless bridge volume and c is a constant equal to 3.6. Expression (1) was found to be in reasonable agreement with the limited amount of available experimental data at the time [2]. In a recent experimental work, Simons *et al.* [4] observed a large spread within their data and concluded that the value of the constant c seems to be dependent on liquid viscosity, whilst the power term is dependent on the bridge geometry (contact angle).

On the other hand, Willett and Seville [5] calculated the dependence of $\tilde{W}_{\rm cap}$ on the contact angle (θ) and proposed a new expression for c, keeping the power term unchanged:

$$\tilde{W}_{\rm cap} \approx \frac{2\tilde{V}^{0.5}}{0.45 - 0.08\theta + 0.3\theta^2}\,. \tag{2}$$

While equation (1) is based on capillary forces only, Ennis *et al.* indicated that if the liquid (binder) is sufficiently viscous, the interaction is dominated by lubrication forces [6]. In this paper, we propose an analytical expression for the rupture energy, taking into account capillary and viscous interactions. The theoretical predictions are compared to accurate measurement results for the force exerted by a pendular liquid bridge between two spheres, in the absence and in the presence of viscous effects. Theoretical considerations are given in the next part, experimental equipment and experiments are presented in part three. The results are then discussed, before we conclude.

[a] e-mail: pitois@univ-mlv.fr

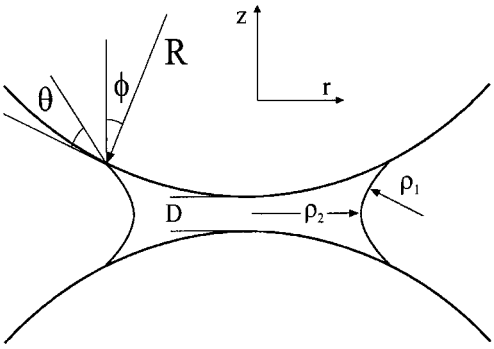

Fig. 1. Liquid bridge between two spheres.

2 Theory

2.1 Capillary adhesion

For small amounts of liquid, gravity effects can be neglected, and the static attractive force due to the meniscus can be expressed as the sum of the capillary force and the axial component of surface tension forces acting on the spheres [7]:

$$F_{\rm cap} = 2\pi R\sigma \sin\phi \sin(\phi+\theta) - \Delta P \pi R^2 \sin^2\phi \qquad (3)$$

where ϕ is the half-filling angle (see Fig. 1). The difference in hydrostatic pressure across the interface (ΔP) is then constant and related to the local mean curvature Γ and to the surface tension by the Young-Laplace equation:

$$\Delta P = \sigma 2\Gamma \qquad (4)$$

where Γ can be expressed as a function of the cylindrical coordinates of the radial profile of the liquid-gas interface:

$$2\Gamma = \frac{1}{r\left[1+(\mathrm{d}r/\mathrm{d}z)^2\right]^{1/2}} - \frac{\mathrm{d}^2 r/\mathrm{d}z^2}{\left[1+(\mathrm{d}r/\mathrm{d}z)^2\right]^{3/2}}. \qquad (5)$$

For given values of θ and V, equation (5) can be solved analytically in terms of elliptic integrals [8] or numerically (see reference [9] for more details about the resolution procedure). One alternative to exact methods is to consider a circular approximation for the meridian profile of the interface. One of them, the "gorge method", gives total forces within 10% of those obtained by means of an exact numerical technique [10]. The force takes then the simple closed-form expression:

$$\left.\begin{aligned} F_{\rm cap} &= \pi\rho_2^2\Delta P + 2\pi\rho_2\sigma = \pi\sigma\rho_2\left[1+\frac{\rho_2}{\rho_1}\right] \\ \rho_1 &= \frac{D/2 + R(1-\cos\phi)}{\cos(\phi+\theta)} \\ \rho_2 &= R\sin\phi - [1-\sin(\phi+\theta)]\rho_1 \end{aligned}\right\} \qquad (6)$$

where ρ_1 and ρ_2 are respectively the radius of the meridian profile and the radius at the neck (see Fig. 1). In equation (6), ϕ has to be determined from geometrical considerations. Following a different approach and in the limit of small liquid volumes, a simplified expression can be derived for the dimensionless capillary force $\tilde{F}_{\rm cap}$ as a function of the liquid volume [11,12]:

$$\tilde{F}_{\rm cap} = \frac{F_{\rm cap}}{\sigma R} \simeq 2\pi\cos\theta\zeta_v, \quad \text{with } \zeta_v = 1 - \left(1+\frac{2\tilde{V}}{\pi\tilde{D}^2}\right)^{-1/2}. \qquad (7)$$

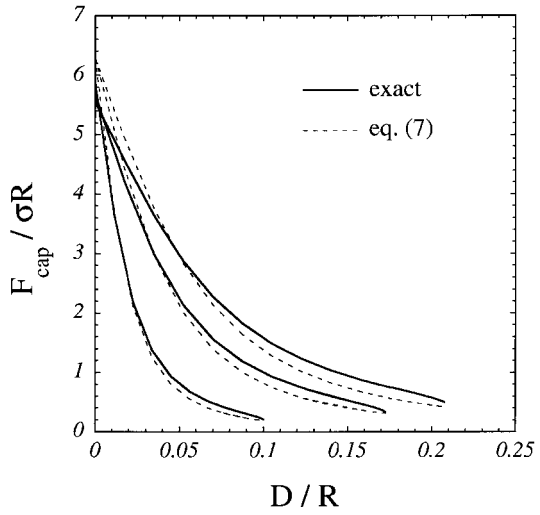

Fig. 2. Evolution of capillary forces with the separation distance. Comparison of equation (7) with numerical results for three bridge volumes (0.001, 0.01 and 0.1).

The values given by equation (7) have been found to be overestimated with respect to exact calculation and experimental results at small separation distances and underestimated at large separation distances [12]. A comparison of the values with numerical results is presented in Figure 2 for three values of the dimensionless bridge volume: 0.001, 0.01 and 0.1. It is shown that equation (7) provides a reasonable approximation for estimating the average force.

The rupture energy $\tilde{W}_{\rm cap}$ can then be calculated by integrating the capillary force with respect to the separation distance, between zero and the quasi-static rupture distance [10]:

$$\tilde{D}^s_{\rm rupt} \simeq \left(1+\frac{\theta}{2}\right)\tilde{V}^{1/3}. \qquad (8)$$

Using (7), the following expression for $\tilde{W}_{\rm cap}$ is obtained:

$$\begin{aligned} \tilde{W}_{\rm cap} &= \int_0^{\tilde{D}_{\rm rupt}} \tilde{F}_{\rm cap}\mathrm{d}\tilde{D} \\ &= 2\pi\cos\theta\left\{(1+\theta/2)(1-A)\tilde{V}^{1/3} + \sqrt{\frac{2\tilde{V}}{\pi}}\right\} \end{aligned} \qquad (9)$$

where A is given by $A = \left(1+2\tilde{V}^{1/3}/\pi(1+\theta/2)^2\right)^{1/2}$.

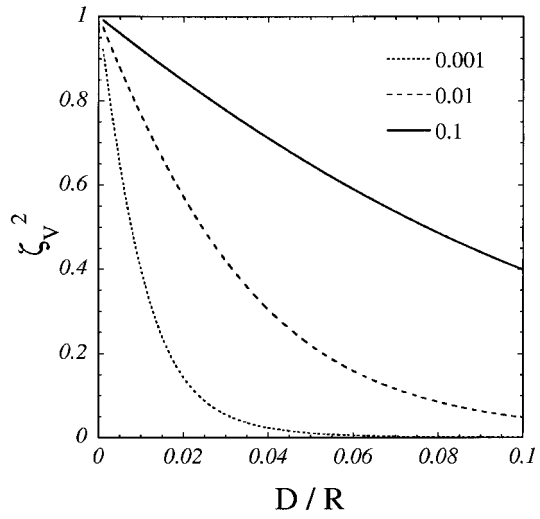

Fig. 3. Evolution of the factor ζ_v^2 with the separation distance for three bridge volumes (0.001, 0.01 and 0.1).

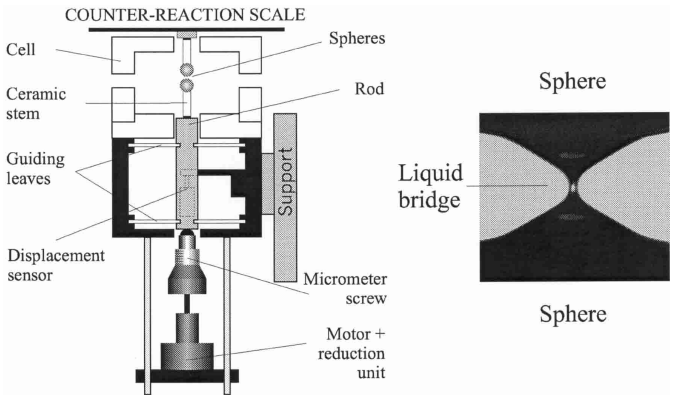

Fig. 4. Experimental liquid bridge apparatus. An image of a bridge of viscous liquid (during the rupture process: see Sect. 4.2) is presented on the right (the bright point in the liquid filament is an optical artefact).

2.2 Lubrication forces

The mechanics of thin liquid films are described by the well-known Reynolds equation, which relates the pressure P generated in the liquid to the relative displacement of the two solid surfaces [13]:

$$\frac{\mathrm{d}}{\mathrm{d}r}\left[rH^3(r)\frac{\mathrm{d}P(r)}{\mathrm{d}r}\right] = 12\eta r\frac{\mathrm{d}D}{\mathrm{d}t} \tag{10}$$

where $H(r) = D + r^2/R$ and η is the liquid viscosity. Integrating twice equation (10) over a distance equal to the radius of the wetted area, the following expression can be derived for the dimensionless attractive viscous force acting on the spheres [12]:

$$\tilde{F}_{\mathrm{visc}} = \frac{F_{\mathrm{visc}}}{\sigma R} = \frac{3}{2}\pi\frac{Ca}{\tilde{D}}\zeta_v^2 \tag{11}$$

where $Ca = \eta\nu/\sigma$ is the Capillary number and ν the spheres velocity (relative displacement). For $\tilde{D}$ close to 0.1, the deviation of the lubrication expression with respect to a higher order analysis [14] is less than 5%. Note that the latter expression differs from the one proposed by Ennis *et al.* [15] by the factor ζ_v^2. Figure 3 presents the evolution of this factor with respect to the dimensionless separation distance for three values of the dimensionless bridge volume: 0.001, 0.01 and 0.1. It is shown that in the case of small liquid amounts, ζ_v^2 (and the related viscous force) is drastically decreased whereas this effect is moderate for larger bridge volumes. Note also that the ratio of viscous to capillary forces is proportional to $Ca\zeta_v/\tilde{D}$.

The viscous impulse is then derived as followed:

$$\begin{aligned}\tilde{W}_{\mathrm{visc}} &= \frac{W_{\mathrm{visc}}}{\sigma R^2} = \int_{\tilde{D}_{\mathrm{m}}}^{\tilde{D}_{\mathrm{rupt}}} \tilde{F}_{\mathrm{visc}}\mathrm{d}\tilde{D} \\ &= \frac{3}{2}\pi Ca\left[\ln\left(\frac{A\sqrt{\pi}}{(1+A)^2}\right) - f(\tilde{D}_{\mathrm{m}})\right] \qquad (12)\end{aligned}$$

$$\text{with}\quad f(\tilde{D}_{\mathrm{m}}) = \ln\tilde{D}_{\mathrm{m}} - 2\ln\left[(\tilde{D}_{\mathrm{m}}) + \sqrt{\tilde{D}_{\mathrm{m}}^2 + \frac{2\tilde{V}}{\pi}}\right] + \frac{1}{2}\ln(\pi\tilde{D}_{\mathrm{m}}^2 + 2\tilde{V})$$

where $\tilde{D}_{\mathrm{m}}$ represents some dimensionless characteristic length scale of surface asperities.

3 Experimental

3.1 Experimental arrangement

An apparatus was constructed for measuring the resultant vertical forces exerted by a viscous liquid meniscus strained between two moving spheres. The main part of this apparatus is schematically shown in Figure 4. The meniscus is formed between two polished ruby spheres of radius $R = 4$ mm (± 1 μm). The upper one is bolted under the arm of a counter-reaction scale (Sartorius MDRA200) which allows the measurement of the vertical force applied to the sphere without displacement of it. Attractive forces can be measured in the range 0–6 N with a precision of 10 μN. The other sphere is bolted to a metallic rod guided along the vertical axis by two planar springs. The rod can be moved up and down by means of a motor-driven differential micrometer screw allowing the increase or decrease of the spheres separation distance at a constant velocity. The separation distance can be adjusted in the range 0–1 mm and the displacement velocities can be varied from 0.01 to 15 μm/s. A displacement sensor tracks the position of the rod with a precision of about 1/4 μm.

Table 1. Properties of the liquids used during the experiments.

Liquids	Surface Tension (mN/m)	Viscosity (mPa s)
1 (PDMS Oil)	21	0.1
2 (PDMS Oil)	21	100

The element described above stands in a large thermostated cell (generally $T = 25 \pm 0.2$ °C). A small thermostated chamber can be used to maintain locally the spheres at a temperature significantly different from the ambient temperature. A lens and a camera (connected to a computer) allow us to save images of the contact region.

3.2 Materials

Bridge materials and related properties (25 °C) are presented in Table 1. The angles of contact of oils with the ruby spheres were found to be in the range 0–10°. The value of θ will be taken equal to 10° in every theoretical evaluation.

3.3 Experimental procedure

First, we measure the position for which contact between spheres is detected (non-zero force detected). This reference position allows us to pull the spheres apart with a known separation distance (D). An amount of liquid is then inserted in the contact region with a syringe. Images of the contact region before and after the formation of the meniscus and some image processing allow the determination of the bridge volume with a precision of about 5%. Several accommodation cycles of spheres approach and separation are generally performed before starting the measurements in order to obtain a perfect axisymmetric bridge.

4 Results and discussion

4.1 Capillary regime

Measurements were performed with liquid 1 during the increase of D at a low rate: $\nu = 0.01$ μm/s. Typical examples of the results obtained for the attractive capillary force are presented in Figure 5 for dimensionless bridge volumes equal to 0.001 and 0.023. The values given by expressions (7) as well as curves corresponding to the exact numerical resolution are also plotted: a close agreement is observed. Best fits of the $\tilde{F} = f(\tilde{D}, \tilde{V})$ plots obtained for several values of the dimensionless bridge volume allow the determination of the rupture energy as a function of $\tilde{V}$. Results are compared to the values given by expression (9) and presented in Figure 6. It is shown that the theoretical values are in very close agreement with the experimental one, reflecting the ability of equation (7) to average the capillary force. Comparisons of equation (9) with exact calculation and expressions proposed by Simons *et al.* (1) and Willett *et al.* (2) are presented in Figure 7 as a function of $\tilde{V}$. It can be seen that our results are in close agreement with the numerical calculation for all dimensionless bridge volumes in the range 0.001–0.1. On the other hand, it can be seen that the power law exponent proposed by Simons *et al.* is above the theoretical average value, close to 0.46. As a consequence, deviations are observed for lower and higher values of $\tilde{V}$ when using equations (1) and (2) respectively. Nevertheless all theoretical values remain close each other, indicating that experimental discrepancies reported by Simons *et al.* seem to result from experimental difficulties in force measurements.

The dependence of the contact angle on the rupture energy is presented in Figure 8. It appears that for every bridge volume considered, equation (9) underestimates the

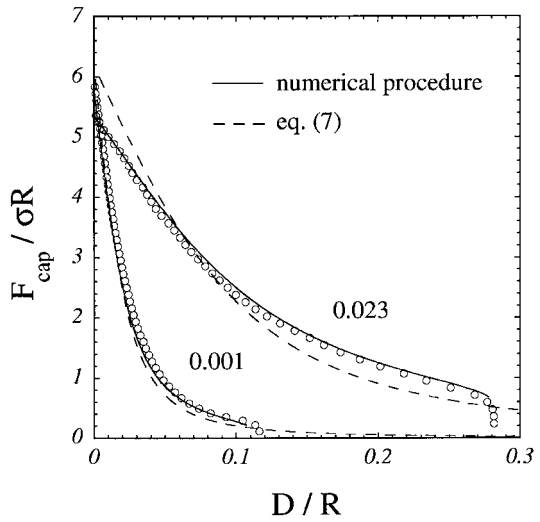

Fig. 5. Evolution of capillary forces with the separation distance. Comparison of experimental results with theoretical values for two bridge volumes (0.001, 0.023).

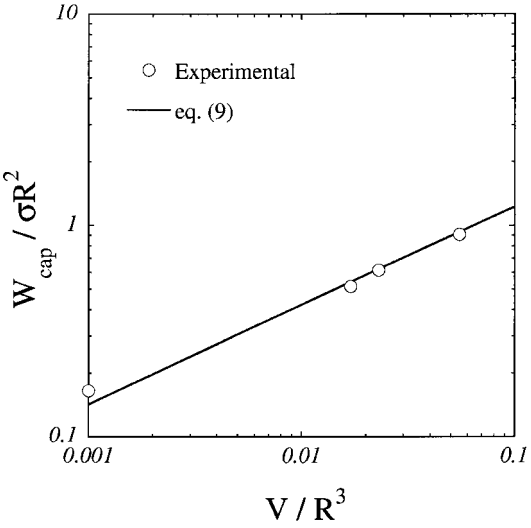

Fig. 6. Rupture energy of a pendular liquid bridge (capillary forces only) as a function of the bridge volume: comparison of experimental results with equation (9).

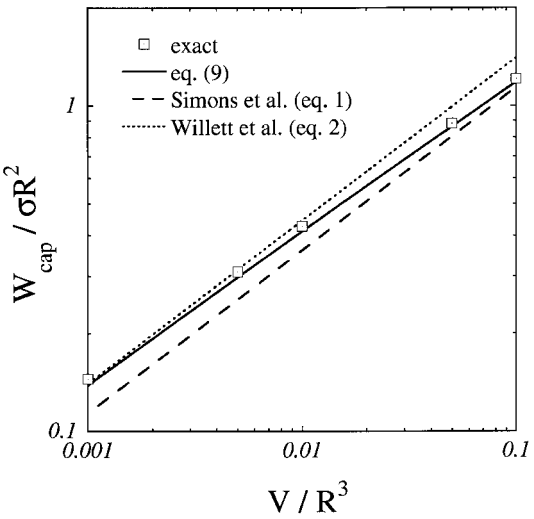

Fig. 7. Rupture energy of a pendular liquid bridge (capillary forces only) as a function of the bridge volume: comparison of equation (9) with equations (1) and (2). The squares represent a numerical evaluation.

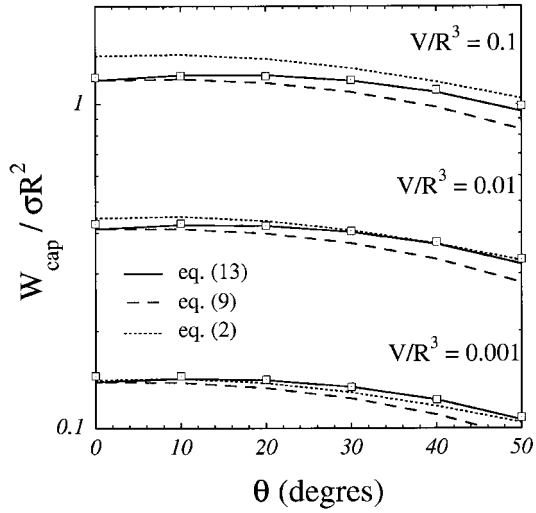

Fig. 8. Rupture energy of a pendular liquid bridge (capillary forces only) as a function of the solid/liquid contact angle for three bridge volumes (0.001, 0.01 and 0.1). The squares represent a numerical evaluation.

numerical results at high θ values. The predictions can be significantly improved by introducing an adjustment coefficient: $(1+\theta/2\pi)$, so that the rupture energy is thus rewritten as followed:

$$\tilde{W}_{\mathrm{cap}} \simeq 2\pi\cos\theta\left(1+\frac{\theta}{2\pi}\right) \times\left\{(1+\theta/2)(1-A)\tilde{V}^{1/3}+\sqrt{\frac{2\tilde{V}}{\pi}}\right\}. \qquad (13)$$

The results presented in Figure 8 indicate that the rupture energy is just weakly dependent on the contact angle, for values below 30°: the increase in bridge rupture distance compensates the decrease of the average capillary force. Besides, a non-monotonic behaviour can be observed.

4.2 Influence of viscosity effects

Results for the attractive force measured during the increase of the separation distance are presented in Figure 9 for a volume of liquid 2 approximately equal to 0.5 μl. The volume of liquid was chosen small enough for the corresponding rupture distance to be smaller than the maximum separation gap (1 mm) for all separation velocities. Note that for $\nu \leq 5$ μm, force measurements corresponding to $\tilde{D} \leq 0.004$ (0.012 for $\nu = 10$ μm) are not presented: with the present equipment, an acceleration slope is required to reach the imposed separation velocity. Figure 9 shows that the viscous forces dominate for the smallest values of $\tilde{D}$ whereas interactions are dominated by capillary forces for the highest separation distances. As reported by several authors [15–17], the dynamic attractive force measured can be several orders of magnitude higher than the corresponding static one. Adding the capillary

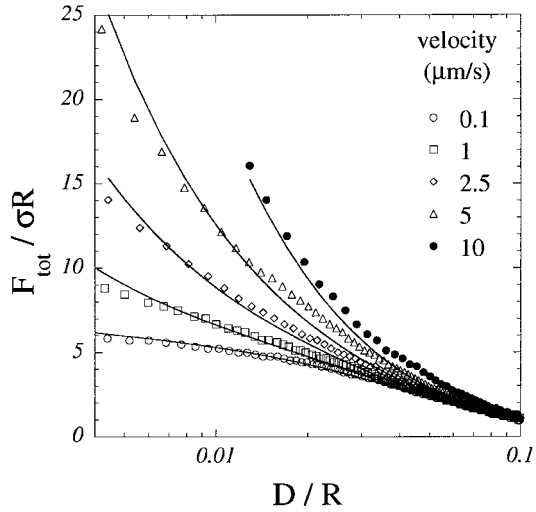

Fig. 9. Evolution of the total attractive force (capillary and lubrication forces) exerted by a liquid bridge stretched between two spheres at a constant velocity. Experimental results are compared with equation (14).

and viscous contributions expressed by equations (7, 11) leads to the simple expression for the total force:

$$\tilde{F}_{\mathrm{tot}} = \tilde{F}_{\mathrm{cap}} + \tilde{F}_{\mathrm{visc}} = 2\pi\cos\theta\zeta_v + \frac{3}{2}\pi\frac{Ca}{\tilde{D}}\zeta_v^2. \qquad (14)$$

Values given by equation (14) are plotted in Figure 9, showing a good agreement with experimental results. Some discrepancies appear at low separation distances, possibly due to the influence of surface asperities. It was checked that these discrepancies can be slightly reduced by introducing an additional effective separation distance $(\tilde{D}+\tilde{D}_{\mathrm{m}})$ in the viscous term expression. Summing the capillary (Eq. (13)) and viscous (Eq. (12)) terms, the total

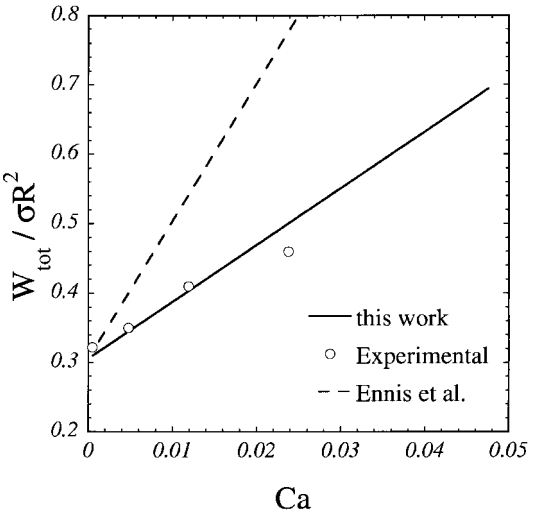

Fig. 10. Evolution of the total rupture energy (including viscous effects) of a pendular liquid bridge as a function of the capillary number: experimental results are compared with equations (15, 16), proposed by Ennis *et al.* [15].

rupture energy expresses as followed:

$$\tilde{W}_{\mathrm{tot}} = \tilde{W}_{\mathrm{cap}} + \tilde{W}_{\mathrm{visc}}. \tag{15}$$

Rupture energies corresponding to the theoretical and experimental curves presented in Figure 9 ($0.004 \leq \tilde{D} \leq 0.1$) have been calculated. Results, presented in Figure 10 as a function of the capillary number, show a good agreement. Deviation observed for the highest value of Ca reflects the slight overestimation of the viscous force at small separation distances. Note that we observed an increase of the bridge rupture distance as a function of the spheres velocity. Nevertheless, as the force contribution is minor at these large separation distances, this effect will not be taken into account at the time and will be considered separately (see end of this section). The rupture energy based on the following expression for the total force [15]:

$$\tilde{F}_{\mathrm{tot}} = \tilde{F}_{\mathrm{cap}} + \frac{3}{2}\pi\frac{Ca}{\tilde{D}} = \pi\tilde{\rho}_2\left[1 + \frac{\tilde{\rho}_2}{\tilde{\rho}_1}\right] + \frac{3}{2}\pi\frac{Ca}{\tilde{D}} \tag{16}$$

is also presented in Figure 10. It can be seen that the use of the latter leads to a significant overestimation with respect to experimental values as soon as viscous effects are present. This appears to result from the drastic influence of the factor ζ_v^2 (see Fig. 3).

Evolution of $\tilde{W}_{\mathrm{tot}}$ given by equation (15) can then be plotted as a function of $\tilde{V}$ for several values of the capillary number. The curves are presented in Figures 11a and 11b for two values of $\tilde{D}_{\mathrm{m}}$: 0.05 and 0.01 respectively. It can be seen in Figure 11a that for $Ca < 1$, viscosity effects become significant for large liquid bridge volumes only, so that a transitional regime is observed. As a result, the power law exponent must be increased in equation (1), while the value of c seems to remain unchanged. This behaviour is opposite to conclusions of Simons *et al.* [4]. As

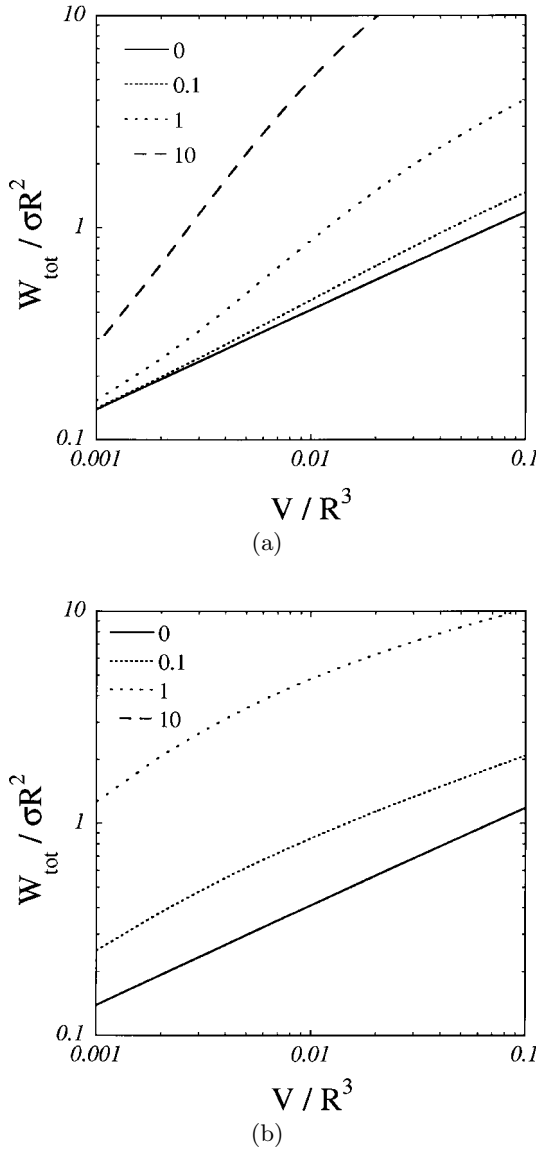

Fig. 11. Evolution of the total rupture energy (including viscous effects) of a pendular liquid bridge as a function of the bridge volume for several values of the capillary number. (a) dimensionless characteristic length scale of surface asperities $\tilde{D}_{\mathrm{m}} = 0.05$ (b) $\tilde{D}_{\mathrm{m}} = 0.01$.

expected, the total rupture energy is efficiently increased as Ca exceeds unity, even for small bridge volumes. The influence of the length scale D_{m} can be assessed by comparing Figures 11a and b: the rupture energy is drastically increased, especially for small liquid bridges, reflecting the diverging behaviour of the viscous force at small separation distances. In addition, it can be seen in Figure 11b that over the volumes range considered, the results can be correctly described by a power law exponent close to 0.5. In contrast with the results obtained for $\tilde{D}_{\mathrm{m}} = 0.05$, this behaviour is in agreement with conclusions of Simons *et al.* [4]: the value of c increases as viscous effects become dominant.

In the presence of viscosity effects, the bridge rupture does not occur instantaneously during the spheres separation process, so that the dynamic bridge rupture distance ($D^d_{\rm rupt}$) can be significantly larger than the corresponding static one. This was qualitatively observed during experiments on liquid bridges between two spheres [18] and quantitatively in the particular case of slender liquid bridges (of moderate viscosity) stretched between two disks moved apart at a relatively high speed [19] (in this case the triple line is fixed on the disks perimeter). Measurement of the evolution of the liquid bridge rupture distance, expressed by:

$$\Delta D_{\rm rupt} = \frac{D^d_{\rm rupt} - D^s_{\rm rupt}}{D^s_{\rm rupt}} \tag{17}$$

is plotted in Figure 12 as a function of Ca. The results, obtained for an intermediate value of in the range 0.001–0.1, clearly indicate that the rupture distance increases as the sphere velocity increases: for $\nu = 10$ μm/s ($Ca \approx 0.05$) ($D^d_{\rm rupt}$), is 20% larger than the corresponding ($D^s_{\rm rupt}$). A power law exponent can be identified over two decades for Ca:

$$\Delta D_{\rm rupt} = Ca^{1/2}. \tag{18}$$

This power law seems to be hardly predictable through simple theoretical considerations. In fact, the rupture mechanism is associated to a complex interface deformation process. The image presented with Figure 4 clearly shows that the bridge rupture proceeds in the formation of a thin liquid filament linking the two volumes of liquid resting on the spheres. Note also the high value of the apparent dynamic solid/liquid contact angle and the particular conical shape of the liquid remaining on each sphere. Nevertheless, the rupture criterion (8) can now be reformulated in the case of a dynamic rupture process:

$$\tilde{D}^d_{\rm rupt} = (1 + \theta/2)(1 + Ca^{1/2})\tilde{V}^{1/3}. \tag{19}$$

5 Conclusion

We performed accurate measurements of the force exerted by a liquid bridge on two spheres separated at a constant velocity, in the absence and in the presence of viscosity effects, in the case of good wetting conditions. In the capillary regime, we proposed an analytical expression (13) for the dimensionless rupture energy of the bridge, expressed as a function of the bridge volume and the contact angle. It has been shown that the values given by this expression are very close to exact numerical calculations and experimental data. These results were also found to be in good agreement with existing curve fitting relations (1, 2).

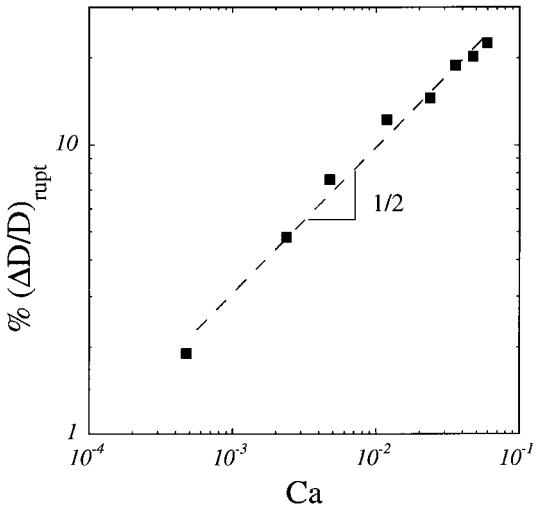

Fig. 12. Increase of the bridge rupture distance ($V = 0.5$ μl) as a function of the capillary number.

In the case of additional viscous effects, we modified expression (13) by adding a viscous term (12) and proposed an analytical expression for the total rupture energy (15). The predictions were found to be in good agreement with experimental data. When plotting the total rupture energy as a function of the capillary number Ca, a linear curve was obtained, the slope of which has been found to be proportional to the factor ζ_v^2. This behaviour is in contrast with rupture energies calculated from the total force expression proposed by Ennis *et al.* [15]. The latter does not take into account the bridge volume dependance and the resulting values significantly overestimate experimental one. With respect to the model proposed by Simons *et al.*, we showed that the value of the parameter c (see Eq. (1)) do not necessary depend on liquid viscosity. In addition, it was shown that the power law exponent proposed by these authors could be significantly increased in the presence of viscosity effects.

The bridge rupture distance was measured as a function of the spheres velocity. We observed that the dynamic rupture distance $\tilde{D}^d_{\rm rupt}$ could be increased with respect to its static counterpart. The increase of the rupture distance was found to be simply related to Ca. In this respect, a modified expression for the rupture criterion proposed by Lian *et al.* [10] has been proposed.

Nomenclature

$\tilde{V} = V/R$ dimensionless bridge volume

σ surface tension

R spheres radius

$F_{\rm cap}$ and $F_{\rm visc}$ capillary and viscous forces

$\tilde{F} = F/\sigma R$ dimensionless force

$W_{\rm cap}$ and $W_{\rm visc}$ capillary and viscous bridge rupture energies

$\tilde{W} = W/\sigma R^2$ dimensionless rupture energy

θ solid/liquid contact angle

ϕ half-filling angle

ΔP difference in hydrostatic pressure across the liquid/air interface

Γ local mean curvature of the interface

r, z cylindrical coordinates

ρ_1 radius of the meridian profile of the liquid/air interface

ρ_2 radius at the neck of the bridge

$\tilde{D} = D/R$ dimensionless separation distance

$\zeta_v = 1 - (1 + 2\tilde{V}/\pi\tilde{D}^2)^{-1/2}$

$\tilde{D}^s_{\rm rupt}$ quasi-static bridge rupture distance

$\tilde{D}^d_{\rm rupt}$ dynamic bridge rupture distance

$A = (1 + 2\tilde{V}^{1/3}/\pi(1 + \theta/2)^2)^{1/2}$

P liquid pressure

η liquid viscosity

$H(r) = D + r^2/R$

ν relative spheres velocity

$Ca = \eta\nu/\sigma$ Capillary number

$\tilde{D}_{\rm m}$ dimensionless characteristic length scale of asperities

$\Delta D_{\rm rupt} = (D^d_{\rm rupt} - D^s_{\rm rupt})/D^s_{\rm rupt}$

References

1. J.R. Johanson, Chem. Technol. **5**, 572 (1975).
2. S.J.R. Simons, J.P.K. Seville, M.J. Adams, Chem. Eng. Sci. **49**, 2331 (1994).
3. R.J. Fairbrother, S.J.R. Simons, in *World Congress on Particle Technology 3* (Institution of Chemical Engineers, 1998), paper 110.
4. S.J.R. Simons, R.J. Fairbrother, Powder Technol. **110**, 44 (2000).
5. C.D. Willett, J.P.K. Seville, in *World Congress on Particle Technology 3* (Institution of Chemical Engineers, 1998), paper 79.
6. B.J. Ennis, G. Tardos, R. Pfeffer, Powder Technol. **65**, 257 (1991).
7. R.A. Fisher, J. Agric. Sci. **16**, 492 (1926).
8. F.M. Orr, L.E. Scriven, A.P. Rivas, J. Fluid Mech. **67**, 723 (1975).
9. D.N. Mazzone, G.I. Tardos, R. Pfeffer, J. Colloid Interface Sci. **113**, 544 (1986).
10. G. Lian, C. Thornton, M.J. Adams, J. Colloid Interface Sci. **161**, 138 (1993).
11. D.J. Maugis, Adhesion Sci. Technol. **1**, 105 (1987).
12. O. Pitois, P. Moucheront, X. Chateau, J. Colloid Interface Sci. **231**, 26 (2000).
13. A. Cameron, *The principles of lubrication* (Longmans, 1964).
14. R.G. Cox, H. Brenner, Chem. Eng. Sci. **22**, 1753 (1967).
15. B.J. Ennis, J. Li, G. Tardos, R. Pfeffer, Chem. Eng. Sci. **45**, 3071 (1990).
16. M.J. Adams, V. Perchard, I. Chem. Eng. Symp. Series **91**, 147 (1984).
17. M.J. Matthewson, Phil. Mag. A **57**, 207 (1988).
18. D.N. Mazzone, G.I. Tardos, R. Pfeffer, Powder Technol. **51**, 71 (1987).
19. X. Zhang , R.S. Padgett, O.A. Basaran, J. Fluid Mech. **329**, 207 (1996).